Exopolymer alteration of physical properties of sea ice and implications for ice habitability and biogeochemistry in a warmer Arctic

Christopher Krembs[a], Hajo Eicken[b], and Jody W. Deming[c,1]

[a]Washington State Department of Ecology, Olympia, WA 98504-7600; [b]Geophysical Institute, University of Alaska Fairbanks, Fairbanks, AK 99775-7320; and [c]School of Oceanography, University of Washington, Seattle, WA 98195-7940

The physical properties of Arctic sea ice determine its habitability. Whether ice-dwelling organisms can change those properties has rarely been addressed. Following discovery that sea ice contains an abundance of gelatinous extracellular polymeric substances (EPS), we examined the effects of algal EPS on the microstructure and salt retention of ice grown from saline solutions containing EPS from a culture of the sea-ice diatom, *Melosira arctica*. We also experimented with xanthan gum and with EPS from a culture of the cold-adapted bacterium *Colwellia psychrerythraea* strain 34H. Quantitative microscopic analyses of the artificial ice containing *Melosira* EPS revealed convoluted ice-pore morphologies of high fractal dimension, mimicking features found in EPS-rich coastal sea ice, whereas EPS-free (control) ice featured much simpler pore geometries. A heat-sensitive glycoprotein fraction of *Melosira* EPS accounted for complex pore morphologies. Although all tested forms of EPS increased bulk ice salinity (by 11–59%) above the controls, ice containing native *Melosira* EPS retained the most salt. EPS effects on ice and pore microstructure improve sea ice habitability, survivability, and potential for increased primary productivity, even as they may alter the persistence and biogeochemical imprint of sea ice on the surface ocean in a warming climate.

ice algae | permeability | polysaccharides | saline ice

Over the past few decades, the extent and thickness of Arctic sea ice have undergone significant climate-driven reductions that show no abatement (1–3). Current polar ecosystems depend on sea ice as a platform for foraging and reproduction by marine organisms and as a porous matrix that supports extensive blooms of ice algae. In the Arctic, these blooms account for a seasonally early and dominant fraction of total spring primary production (4). With continued reductions in areal extent of summer sea ice, however, phytoplankton activity in open waters is expected to dominate total primary production (5), leading to shifts away from ecosystems supported by fluxes of ice-algal material to the seafloor (6) toward pelagic ecosystems characteristic of lower latitudes (7). Predictions of reduced ice-algal production, however, do not consider the possibility that changes to sea ice microstructure and physical properties may stimulate primary productivity in the remaining ice.

Here we reframe the question of how large-scale losses of Arctic sea ice will impact ecosystems and ask instead whether organisms—in particular sea-ice algae—have evolved means to alter ice physical properties to their benefit, mitigating impacts of climate change. The mechanism we consider derives from the biological production of extracellular polysaccharide substances (EPS)—organic materials of high surface area and complex behavior in aqueous solution (8)—observed microscopically in the brine inclusions of sea ice, where they are thought to function as cryoprotectants (9) and osmoprotectants (10). Do these substances also alter the microstructure of the pore space inhabited by ice algae, changing ice permeability and convective exchange with water below the ice? EPS influence physical phenomena of large-scale significance in other natural settings, including hydraulic and mechanical properties of porous media (11), cohesion of aquatic sediments (12), and water and solute retention in rocks and soils (13). However, their potential to alter sea-ice properties has not been addressed (14), despite the abundance of EPS in ice (9) and the importance of sea ice in a global context.

Earlier, we suggested that the presence of EPS, which dominate (9, 15) the millimolar amounts of organic carbon measured in sea ice (16), may modify pore space or interfere with salt expulsion from growing ice, leading to higher ice porosities and salinities (9, 10). Here, we have tested this hypothesis via detailed microscopic observations of the brine inclusions in well-characterized coastal sea ice (Barrow, AK) near the growing ice front and in laboratory ice grown from saline solutions with and without added EPS, coupled with measurements of salt retention. Anticipating differences between EPS present in natural sea ice and EPS used in experimental work, we moved beyond conventional use of the Alcian blue (AB) staining technique (17) for quantifying large-sized gelatinous EPS (9) and applied the phenol/sulfuric acid (PSA) assay based on sugar-monomer content (18) and a density gradient approach to evaluate size-fractionated EPS. A full chemical characterization of sea-ice EPS remains elusive, but measurements of high uronic acid content (19) confirm the gelling properties that increase fluid viscosity (8) and the likely presence of protein moieties (common in culture-derived EPS; ref. 20), and specifically glycoproteins, suggests the capacity to alter the morphology of growing ice crystals (21).

For our ice-growth experiments, we harvested EPS from *Melosira arctica* var. *krembsii*, a diatom species long known to produce copious amounts of mucus (22). The effects of *Melosira* EPS on brine-pore microstructure were examined for ice grown from saline solutions containing fresh EPS or EPS first exposed to heat and/or enzymatic treatment, the latter specifically to degrade glycoproteins. To test EPS effects on salt retention, we also grew ice from saline solutions with xanthan gum (XG)—the reference standard for EPS in the marine environment (17)—and EPS from a culture of the marine bacterium *Colwellia psychrerythraea* strain 34H, a cold-adapted species found in sea ice.

Results

EPS in the Bottom Layer of Natural Sea Ice. Relatively high amounts of EPS were detected in the bottom decimeter of the sea ice collected (Table S1). By the AB method, the average amount of particulate EPS (pEPS) exceeded the earlier maximum similarly obtained for sea ice in this region: 9.5 ± 1.5 SD ($n = 9$) vs. 7.7 mg·XGequiv·L^{-1} (9). Use of the PSA method (18)—enabling

---

ENVIRONMENTAL SCIENCES

analysis of both pEPS and smaller-sized, previously overlooked polymers here operationally defined as dissolved EPS (dEPS; <0.4 μm)—indicated that the total amount of EPS in this ice was 12 ± 3.3 SD mg·XGequiv·L^{-1} ($n = 9$). The pEPS fractions accounted for 17–42% of the total (Table S1), a unique assessment for sea ice. These fractions are likely higher, as the PSA assay underestimated pEPS relative to the AB method (Table S1), the latter being sensitive to gelatinous material that includes more than sugars. These natural EPS were also more complex in size-based composition than suggested by a single filtration step, given the four major peaks between 3.0 and 183 kDa and a larger, unresolved fraction (>336 kDa) observed by the PSA assay after density gradient fractionation (Fig. S1).

Although the AB method indicated a uniform distribution of pEPS in the ice, which is in line with other studies using this approach (9, 19), the PSA method detected more pEPS near the growing ice front (Table S1). Measures of algal biomass [chlorophyll a and phaeopigments, particulate organic carbon (POC), and particulate nitrogen (PN)] were also elevated near the ice–water interface (Table S2), reflecting the ability of ice algae to follow the moving ice front for nutrient replenishment from underlying waters, while leaving a trail of EPS throughout the ice (9). Ratios of pigments, POC and PN, and macronutrients all indicated a typical, spring ice-algal bloom near the ice–water interface (Table S2). We selected an ice layer containing high concentrations of both pEPS and dEPS at ~3 cm from the ice–water interface (Table S1) for detailed microscopic analyses.

Microscopic Observations of Pores in Natural Sea Ice. When stained and examined at low magnification (Fig. S2), the brine inclusions (pores) of this natural ice were arranged in subparallel arrays, typical of Arctic congelation ice (14). Observations of the pores at high magnification (Fig. S2) revealed that the majority (52%) contained visibly stained EPS (Table S3)—an underestimate, as

stain may not have diffused into all pores or made all EPS visible. Pores with visibly stained EPS were more likely to contain diatoms (Fig. S2) and detritus than pores devoid of stained EPS (Table S3). Most pores filled with stained EPS were highly angular and convoluted in shape; the frequency of such complex morphologies decreased for pores only partially filled or devoid of visibly stained EPS (Table S3). Measuring specific dimensions of these natural EPS-containing brine inclusions confirmed the fractal pore geometries. A log–log plot of pore perimeter vs. maximum length revealed significant deviations, beginning at lengths of ~250 μm, from a power-law relationship of the Euclidian geometries of pores in experimentally grown EPS-free ice (Fig. 1).

Melosira EPS Effects on Microstructure of Tank-Grown Ice. For ice grown from saline solutions containing fresh *Melosira* EPS, observations of stained sections at low magnification revealed fine-grained congelation ice with mostly intergranular brine inclusions of irregular convoluted shape and poorly ordered arrangement (Fig. 2 B, D, and F), closely resembling natural sea ice (ref. 14; Fig. S2). In contrast, ice grown from EPS-free saline solutions was more coarse-grained, with more ellipsoidal brine inclusions and a greater number of lamellar crystal features and lamellar inclusions (Fig. 2). Image analysis of EPS-free ice (Fig. 2C) and ice containing *Melosira* EPS (Fig. 2D) indicated a greater abundance of pores in the EPS-containing ice by as much as 15%. Observations of pores in tank-grown ice at high magnification indicated fractal geometries similar to those in natural sea ice, again deviating at pore lengths ≥250 μm from the power-law function derived from pore dimensions of the control ice (Fig. 1).

EPS Effects on Salinity of Tank-Grown Ice. In tests for salt retention, ice grown from saline solutions containing *Melosira* EPS had higher bulk salinities—by 12–35% (horizon by horizon)—than ice grown in the control tanks (Fig. 3). In the first of three
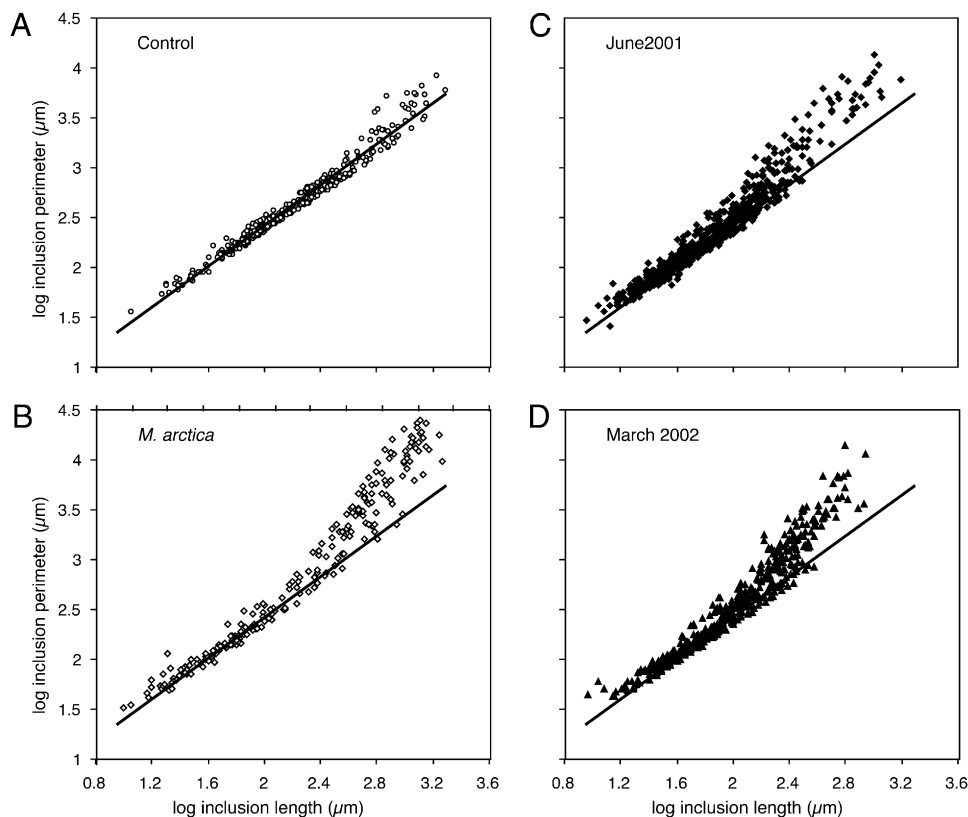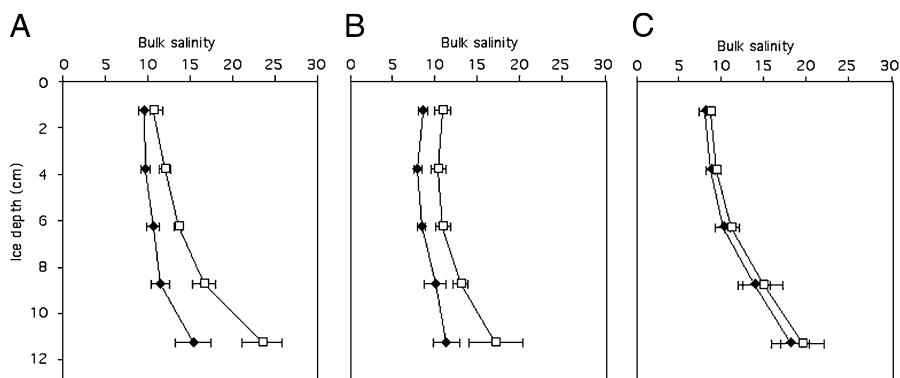

Fig. 1. Comparative relationships between the perimeter and length ($\log_{10}$ μm) of brine inclusions (pores) observed microscopically in artificial sea ice, with and without EPS, and in natural sea ice. (*A* and *B*) Artificial ice was grown from saline solutions with no EPS added (*A*; control, $n = 476$) or *Melosira* EPS added (*B*; *M. arctica*, $n = 234$). (*C* and *D*) Natural sea ice was collected in June 2001 (*C*; $n = 834$) and March 2002 (*D*; $n = 491$). The solid line in each image is a regression fit of the data from the control ice (*A*), where $y = 1.02x + 0.38$ and $r^2 = 0.97$.
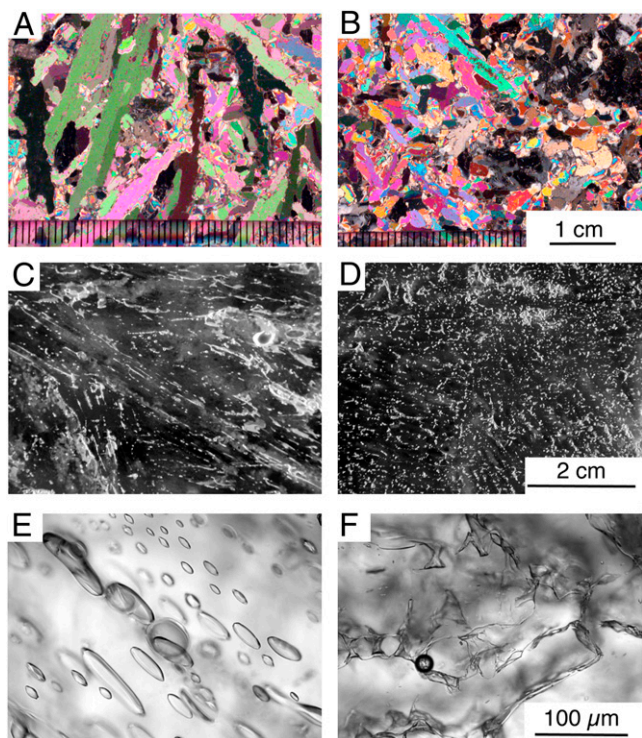
Fig. 2. Photomicrographs at −10 °C of artificial sea ice, with and without EPS. Images show ice texture in horizontal sections (5-cm depth) at low magnification under polarized light (*A* and *B*) and with contrast staining (*C* and *D*), and pore structure at high magnification (*E* and *F*). The ice was grown from saline solutions with no added EPS (*A*, *C*, and *E*) or with *Melosira* EPS (*B*, *D*, and *F*).

experiments (Fig. 3*A*), this horizon-by-horizon difference in bulk salinity increased linearly (4.0% cm^{-1}, $r^2 = 0.97$) and significantly (Spearman rank correlation, $\rho = 1, n = 5, P = 0.045$) with depth in the ice, the greatest difference being at the ice–water interface. In the second (refreeze) experiment (Fig. 3*B*), similar effects on salt retention were apparent, although the depth-dependent salinity difference was not significant. In the third experiment (Fig. 3*C*), where the EPS-containing solution had first been heated, no influence on salt retention was detected (elevated salt content is due to removal of freshwater in the form of ice during each sampling cycle). The amount of *Melosira* EPS in the ice horizons of these three experiments varied (between 16 and 57 mg·XGequiv·L^{-1}), but differences in mean values for a given horizon between experiments were not significant (two-sample *t* test assuming equal variances; $n > 39$).
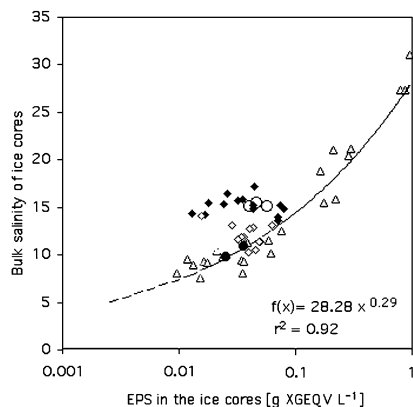
When ice was grown from *Melosira* EPS-containing solution in parallel with large-scale experiments using a range of XG concentrations, the potency of fresh *Melosira* EPS for salt retention was again evident: Mean bulk salinity of the *Melosira* EPS-containing ice exceeded that in EPS-free control ice by 45% (27–57% by horizon), whereas mean bulk salinities of the XG-containing ice exceeded control ice by 11–19% (Table S4). Even the highest starting concentration of XG in these comparative experiments (25-fold higher than in the *Melosira* EPS tank) did not lead to as much salt retention as *Melosira* EPS. Ice grown from solutions containing *Colwellia* EPS also had higher bulk salinities than control ice (Table S5), but by percentages of 17–18%, similar to XG-containing ice.

Relationship Between Salinity and EPS in Tank-Grown Ice. To examine the relationship between salinity and EPS across all ice-growth experiments, we calculated depth-averaged values for the full ice thickness in each tank. A strong functional relationship between the two variables was observed for XG, with data for *Colwellia* EPS closely following the salinity–XG relationship (Fig. 4). The salinity–EPS relationship for heat-treated *Melosira* EPS (Fig. 3*C*) also resembled that of XG and *Colwellia* EPS (Fig. 4), both of which had been exposed to protein-denaturing temperatures during preparation (*SI Materials and Methods*).

In contrast, more salt was retained in ice grown from solutions containing fresh *Melosira* EPS than from those with comparable amounts of any other type of EPS (Fig. 4). Instead of a concentration dependency between salinity and fresh *Melosira* EPS, however, this global graphical analysis indicated a saturation effect (Fig. 4). The difference between salinities of ice with fresh *Melosira* EPS and ice with other types of EPS at the same EPS concentration was strongest at the lower end of the EPS scale (nearly twice as much salt retained)—where EPS values align with those for natural sea ice (Table S1)—and weakest (only a fractional difference) at the higher EPS values. Such a saturation effect would be expected (given finite pore surface area) for EPS that included ice surface-active compounds.

Enzymatically Altered *Melosira* EPS Effects on Pore Microstructure. Given the observed impacts of protein-denaturing temperature on the ability of *Melosira* EPS to enhance salt retention (Figs. 3 and 4) and the alteration of individual ice crystals by glyco-proteins (21), we considered that glycoproteins in *Melosira* EPS may have contributed to observed physical changes in the ice. Results from ice-growth experiments that included *Melosira* EPS first treated enzymatically to denature glycoproteins strongly implicated glycoproteins in microstructural alterations of the ice. The greatest pore complexity was observed for ice containing fresh *Melosira* EPS, and the simplest morphologies were seen for ice containing enzymatically treated *Melosira* EPS (Fig. 5). Neither the enzyme-free control nor treatment of *Melosira* EPS

Fig. 3. Vertical profiles of bulk salinity of ice grown in 13-L tanks at −10 °C from saline solutions with (□) or without (◆) *Melosira* EPS. The first experiment (*A*) was repeated by thawing the unsampled ice and refreezing the entire contents of the tank (*B*). For the third experiment (*C*), the contents were heated to 100 °C for 10 min before refreezing. Ice-growth rates were similar in *A*, *B*, and *C* (0.13–0.15 cm·h^{-1}). Error bars indicate SD of the mean ($n = 3$).

Fig. 4. Comparative relationships between bulk salinity and total EPS content (ice depth-averaged, in XGequiv·L⁻¹) for all ice-growth experiments. Starting solutions contained XG (△), *Colwellia* EPS (●), *Melosira* EPS (13-L tanks, ◆; 200-L tanks, ○), or heat-treated (100 °C) *Melosira* EPS (◇). XG and *Colwellia* EPS had been exposed to 90 °C during preparation. The dashed portion of the functional line for XG (n = 24) is an extension to the lowest observed bulk salinity for natural sea ice in this study.

at 75 °C—a nondenaturing temperature for proteins structurally protected by hydrocolloids and gums (23)—caused a shift away from the distinctively complex pores created by fresh *Melosira* EPS; the EPS-free control presented a neutral pattern by comparison (Fig. 5).

Discussion

Generality of Observations. Data on pigments, particulate organic materials, and nutrients (Table S2) of the sampled ice fell within the range of typical Arctic springtime values (9, 24). We focused on the bottom layer for its significance to Arctic sea-ice productivity (4), the presence of high amounts of EPS (9), and the expectation that EPS effects on ice properties would be most evident in this transition zone between the ice–water interface and solid interior ice. This expectation was met, and our experimental approach was validated by the strong similarities in pore microstructure between ice grown from solutions containing fresh *Melosira* EPS and natural sea ice (Figs. 1 and 2F and Fig. S24; refs. 9 and 14) and the clear distinctions from EPS-free control ice (Figs. 1 and 2E). The microstructural contrasts were striking, despite having to examine the ice at a lower temperature (−10 °C) than its in situ temperature (−2 to −3.5 °C). Warmer bottom ice is destined to become colder interior ice as the ice grows, giving results at −10 °C direct relevance to the winter–spring Arctic sea ice cover. Although our evaluation of EPS effects on salt retention in ice relied upon controlled experimental work, the observed increases in bulk ice salinity were also clear, particularly as mediated by fresh *Melosira* EPS (Figs. 3–5). *M. arctica* represents the EPS-producing diatoms that dominate sea-ice biota across the Arctic, lending generality to the potent effects of its EPS on physical properties of sea ice and consequent implications.

EPS Effects on Physical Properties of Ice. Sea-ice growth is well understood from theory and laboratory experiments at starting salinities of 30–35 (14, 25), as in our EPS-free control experiments. As the ice grows, solutes in the source water are rejected from the solid ice matrix, accumulating near the ice–water interface. The ensuing brine density gradients drive convective exchange with the underlying water (25), typically removing 75–85% of the salt, such that bulk salinities in interior ice layers range between 4 and 10 (14). Most of the brine retained is segregated into lamellar inclusions, several hundred micrometers wide, extending in subparallel arrays through columnar crystals several centimeters long (Fig. 2 A and C).
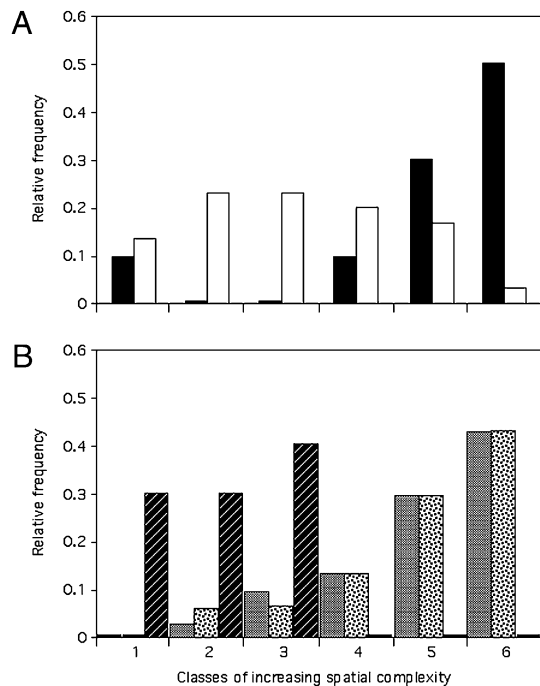
Fig. 5. Relative frequency of images of ice-pore microstructure, sorted according to increasing morphological complexity. Ice was grown from saline solutions with (filled bars) or without (open bars) fresh *Melosira* EPS added (A) or with heat-treated *Melosira* EPS (at 37 °C, gray bars; at 75 °C, dotted bars) or enzyme-treated *Melosira* EPS (glycosidase to denature glycoproteins at 37 °C) added (hatched black bars) (B). Each bar indicates number of images per complexity class as a fraction of total images per treatment.

This study clearly indicates that EPS, if present in sufficient quantity and quality, alter the microstructure and desalination of growing ice. The particularly potent exopolymers of *M. arctica* led to more disordered ice crystals (Fig. 2B), greater pore density (Fig. 2D), more complex pore geometries (Figs. 2F and 5), and greater salt retention by the newly formed ice (Figs. 3 and 4). The mechanisms underlying these effects can be understood by considering EPS behavior in relation to ice permeability, brine viscosity, and ice–surface interaction.

Sea-ice permeability controls bulk flow and depends on porosity and pore microstructure (14); in Darcian pipe flow, permeability scales with the inverse of the square of tortuosity. Fresh *Melosira* EPS clearly altered pore morphogenesis in our artificial ice, leading to convoluted pores and hence greater tortuosity. Were total porosity and pore size unchanged, increases in tortuosity alone would significantly reduce permeability (e.g., a threefold increase in tortuosity, not unlike that observed, would lower permeability by nearly an order of magnitude). Fresh *Melosira* EPS (and XG and *Colwellia* EPS to lesser degrees), however, also caused fractional increases in ice porosity (Fig. 2D) and salt retention (12–59%). Although these increases alone would lead to higher permeability, scaling issues indicate their insufficiency to reverse the effects of increased tortuosity, such that the overall effect of EPS on the ice was to reduce permeability and retain more salt.

The most parsimonious explanation for this result is pore clogging by EPS (10). The natural EPS we examined featured a broad spectrum of size fractions (Fig. S1), including aggregates sufficient to plug pore passages (Fig. S2). Evidence of elevated pEPS near the growing ice front in both natural and tank-grown ice (Table S1) evokes clogging in a zone of otherwise high salt fluxes (14). In this same zone, diatoms were more likely to be retained in a pore even partially filled with EPS than one devoid

of this gelatinous material (Table S3). In other environments, pore clogging by microbially produced EPS explains substantial reductions in the permeability of sediments (26) or of terrestrial soils subjected to freeze–thaw cycles (27). In growing sea ice, pore clogging would impede the desalination process while enhancing retention of organisms within the ice where light levels support substantial algal activity (9).

The presence of gelatinous sugar-based polymers in other systems increases viscosity of the bulk fluid (28) and thus reduces advection and diffusion of ions by up to two orders of magnitude (29). Studies with XG (30) suggest that for shear rates representative of fluid motion in sea ice and for the polymer concentrations we used, an order of magnitude increase in brine viscosity can be expected. Although permeability exerts primary control on desalination, such increases in viscosity can greatly reduce convective–diffusive exchange and contribute to observed higher bulk salinities.

EPS impacts on ice permeability and brine viscosity would be accentuated at the advancing ice–water interface where ionic impurities accumulate (14), as should polysaccharides (31). The depth dependency of the salinization effect observed in our experiments (Fig. 3) supports this idea. If the EPS present in freezing seawater or produced within the ice contains components capable of interacting directly with the surfaces of ice crystals, then the presence and accumulation of EPS at the advancing ice front may also influence ice growth. Although similar ice-growth rates were achieved across experiments through similar growth conditions, a reduced ice-growth rate was observed in the presence of *Melosira* EPS relative to XG and control ice in the outdoor tank experiments (0.1 vs. 0.25–0.3 cm·h^{-1}; Table S4). This result requires further investigation, but, like the saturation effect observed in the global analysis of experimental results (Fig. 4), it is consistent with evidence that *Melosira* EPS contains components, enzymatically deduced as glycoproteins, responsible for the geometric complexity of the ice microstructure (Figs. 1, 2, and 5). If these components prove to be ice-active glycoproteins similar to antifreeze glycoproteins produced by algae from Antarctic sea ice (21), they would be expected to influence ice-growth rate by suppressing development of crystal faces typically found in sea ice (32).

Broader Implications in a Warming Climate. Exopolymer-enhanced retention of salt in growing sea ice translates to greater retention of other source water impurities, including EPS-producing microalgae (15). The benefits of ice entrainment to algae include stable positioning to capture more light energy for photosynthesis and refuge from predation. Sea-ice primary productivity is expected to increase in a warming climate until the nutrient supply from below becomes limiting (4). By altering ice physical properties, EPS precondition the bottom ice layer for optimal habitability, as well as for later survival as the growing ice front becomes colder interior ice with smaller pores of more concentrated brine and biologically protective EPS (9). The survival benefits extend to Bacteria and Archaea ubiquitous in cold winter ice (33). For filamentous ice algae that cross the ice–water interface, accessing nutrients in underlying waters, the EPS-mediated geometric complexities of the ice pore space may help anchor filaments (10), as observed in the natural ice examined (Fig. S2).

As the Arctic sea ice cover has receded in areal extent, the season for primary production in open waters has expanded (5). Secondary fall blooms characteristic of lower latitudinal seas—and already of some Arctic polynyas (34)—will increase in frequency and magnitude. With late-season blooms come higher EPS concentrations in surface waters destined to freeze and thus potential amplification of the EPS effects observed here. The marked effects of our experimental concentrations of EPS, which started at the upper end of the range in natural sea ice (Fig. 4), should thus increase in their relevance to sea ice in coming years.

Sea ice that retains more salt will also retain more of the dissolved constituents of the source water, from carbon dioxide and other greenhouse gases (35) to iron and other nutrients essential to primary production (36). Their retention, alteration, and eventual release determine the biogeochemical imprint of sea ice on the surface ocean (and atmosphere). The reduction of ice permeability by EPS must also influence the role of sea ice as an inorganic carbon pump from atmosphere to underlying ocean (37), as well as its seeding and fertilization of surface waters during the melt season. EPS-targeted studies are needed to quantify these effects.

Although this study has provided clear evidence that EPS alter the growing sea-ice matrix, the impacts of EPS on the melting of ice remain to be documented. The mechanical strength of sea ice depends on salinity (14), with saltier ice, as generated from EPS-rich source waters, being weaker. The persistence of sea ice, however, and its rate of melt reflect a complexity of factors, including that clogged pores and EPS-coated ice surfaces may retard the advection of warmer saline water and reduce melt rates (Fig. S3). Such a potential positive feedback to ice persistence would be of considerable importance to primary production in the ice, its dependent ecosystem, and the ultimate fate of ice in a warming climate. Answering this question requires more investigation, but a potent biological mechanism worth exploring further for its alterations of the physical properties of sea ice has been identified.

Materials and Methods

Collection and Processing of Natural Sea Ice. First-year sea ice was collected with a 10-cm-diameter ice corer in June 2001 (10 cores; Elson Lagoon, 71.3538° N, 156.5195° W; ice thickness of 1.62 m) and March 2002 (5 cores; Chukchi Sea, 71.3285° N, 156.6899° W; ice thickness of 1.57 m). The bottom 10 cm of the cores, originally at −2 to −3.5 °C, were cut on site and placed in sterile polyethylene bags. Some sections were infused with 0.2-μm-filtered isothermal and isohaline AB solution (9), ensuring diffusion into the brine network for later microscopic analyses. Stained and unstained sections were transported at −20 °C (preventing brine drainage) to the cold laboratory at the Geophysical Institute (GI), University of Alaska Fairbanks. Remaining 10-cm samples were cut into eight 1.25-cm sections, bagged, and melted at 0 °C in the dark. Meltwater subsamples were processed for EPS and for POC, PN, chlorophyll *a*, phaeopigments, and dissolved nutrients by using standard methods (Table S2). Meltwater salinity was measured conductometrically at room temperature.

EPS Analysis. To quantify pEPS in natural sea ice, the particulate fractions of 5-mL subsamples of meltwater were collected on 0.4-μm Nuclepore filters, stained with 0.2-μm-filtered AB solution, rinsed, and analyzed as described (9). Additional filters and filtrate (for dEPS) were extracted for analysis by the PSA method (18). All samples were shipped and stored in 5-mL polycarbonate tubes at −20 °C. For artificial ice, pEPS and dEPS were quantified by the PSA method. Spectrophotometric measurements of AB-stained samples were calibrated against XG (17), and those of PSA extracts were calibrated against D-glucose (18). A PSA calibration of XG against glucose enabled expression of all EPS values in XG equivalents (XGequiv). A UV/Vis Perkin-Elmer Lambda2S spectrometer, calibrated against sulfuric acid at 490 and 787 nm, was used in all cases.

Microscopic Analysis of Ice Microstructure and Brine Inclusions. Ice was observed microscopically in transmitted light with a Zeiss Axioskop 2 microscope at −10 °C in the GI laboratory (9), which paralleled outdoor tank temperature and prevented brine drainage from the ice. A contrast agent, titanium dioxide-oil emulsion, was used to differentiate solid ice from brine inclusions (38). To visualize AB-stained EPS, an in vivo approach was applied to microtomed 5-mm sections of ice (9). Photomicrographs of individual brine inclusions were taken from 10 μm below ice surface to a depth of 400 μm. Images were digitized to 256 gray levels and analyzed using a variant of NIH Image. Pore dimensions of maximum length, perimeter, and AB-stained area were measured at 1,143× magnification.

Ice-Growth Tank Experiments for Ice Microstructure and Salt Retention. Ice-growth experiments were conducted in polyethylene-lined tanks at the GI: 13-L tanks in the cold laboratory at −10 °C (for *Melosira* and *Colwellia* EPS)

and 200-L outdoor tanks during winter (for XG), when air temperature fluctuated between −5 and −15 °C. Enough *Melosira* EPS was generated for a 200-L outdoor tank experiment at the same time. Tank sides were insulated with foam, and tops were left open for downward ice growth. Ice-growth rates were determined by recording ice thickness at 12-h intervals with a cross-bar wire gauge.

After ice thickness reached 12.5–13 cm in 13-L tanks with *Melosira* EPS, the ice was subsampled vertically with a band saw, equilibrated at −10 °C, and cut into 2.5-cm horizontal sections (*n* = 12 per depth). Some sections were kept frozen for microscopic analyses; others were melted at 0 °C and analyzed for EPS content and salinity. Ice thickness reached 14 cm in 200-L tanks before subsampling (*n* = 7 per depth) and 5 cm in 13-L tanks with *Colwellia* EPS (*n* = 12 per depth).

Preparation of EPS and Starting Solutions for Tank Experiments. The diatom, *Melosira arctica* var. *krembsii*, was grown to high density at −1.9 °C in nutrient-amended artificial seawater and allowed to settle (*SI Materials and Methods*). EPS-rich water, called "*Melosira* EPS," was siphoned off for use in tank experiments. For 13-L tanks (Fig. 3), the starting solution was artificial seawater, salinity of 30, amended with *Melosira* EPS to 75 mg·XGequiv·L^{-1}; the control tank received no EPS. After ice was subsampled, remaining ice (and solution) was left to thaw at 0 °C. Tanks were incubated again at −10 °C, resulting ice was subsampled, and remaining ice was left to thaw as before. Before ice growth a third time, tank contents were heated at 100 °C for 10 min. For the 200-L tank (Fig. 4), *Melosira* EPS was amended to 7.9 mg·XGequiv·L^{-1}.

For XG experiments, a stock solution of XG was diluted stepwise into NaCl solution and adjusted to 200 L and salinity of 30 (*SI Materials and Methods*). Three tanks were amended with XG of increasing concentration (Table S4); a control tank received no XG. A second set of experiments used twice the amount of XG per tank. "*Colwellia* EPS" was prepared from spent culture

medium of *C. psychrerythraea* strain 34H by a series of ethanol precipitations (*SI Materials and Methods*). Ethanol was removed by evaporation at 90 °C before use to exclude effects on ice growth. Starting solutions were artificial seawater, salinity of 30, with and without added *Colwellia* EPS (Table S5).

Ice-Growth Experiment on Glycoprotein Effects. Fresh *Melosira* EPS were incubated with glycerol-free *N*-glycosidase F, an enzyme that hydrolyzes nearly all types of *N*-glycan chains of glycoproteins; the glycoprotein fraction was deactivated for 10 min at 37 °C (*SI Materials and Methods*). Other aliquots of *Melosira* EPS were incubated without glycosidase for 10 min at 37 °C or at 75 °C. Starting solutions of NaCl, salinity of 30, were amended with the differently treated EPS preparations. Three 0.7-L circular polycarbonate containers per treatment and control were placed in an insulated seawater bath at −2 °C in the GI laboratory at −10 °C, ensuring downward freezing from the top. After ice growth to 10 cm, remaining solution was removed, and the ice was allowed to equilibrate at −10 °C. Then, 5-mm sections were cut at the 5-cm horizon and examined at 60× magnification. For each treatment and control, 140 images of pore structures were assigned random numbers and sorted into classes of increasing spatial complexity, dividing first into two bins according to clear similarity or dissimilarity to control ice, then repeating the process. Images in the last classes, where differences were minor, were merged with their adjacent bins, resulting in six classes of 15–34 images each.

1. Stroeve J, Holland MM, Meier W, Scambos T, Serreze M (2007) Arctic sea ice decline: Faster than forecast. *Geophys Res Lett* 34:L09501.
2. Maslanik JA, et al. (2007) A younger, thinner Arctic ice cover: Increased potential for rapid, extensive sea-ice loss. *Geophys Res Lett* 34:L24501.
3. Nghiem SV, et al. (2007) Rapid reduction of Arctic perennial sea ice. *Geophys Res Lett* 34:L19504.
4. Gradinger R (2009) Sea-ice algae: Major contributors to primary production and algal biomass in the Chukchi and Beaufort Seas during May/June 2002. *Deep Sea Res Part II Top Stud Oceanogr* 56:1201–1212.
5. Arrigo KR, van Dijken G, Pabi S (2008) Impact of a shrinking Arctic ice cover on marine primary production. *Geophys Res Lett* 35:L19603.
6. Forest A, et al. (2008) The annual cycle of particulate organic carbon export in Franklin Bay (Canadian Arctic): Environmental control and food web implications. *J Geophys Res* 113:C03S05.
7. Grebmeier JM, et al. (2006) A major ecosystem shift in the northern Bering Sea. *Science* 311:1461–1464.
8. Decho AW (1990) Microbial exopolymer secretions in ocean environments: Their role (s) in food webs and marine processes. *Oceanogr Mar Biol Annu Rev* 28:73–153.
9. Krembs C, Eicken H, Junge K, Deming JW (2002) High concentrations of exopolymeric substances in Arctic winter sea ice: Implications for the polar ocean carbon cycle and cryoprotection of diatoms. *Deep Sea Res I* 49:2163–2181.
10. Krembs C, Deming JW (2008) The role of exopolymers in microbial adaptation to sea ice. *Psychrophiles: From Biodiversity to Biotechnology*, eds Margesin R, Schinner F, Marx J-C, Gerday C (Springer, Heidelberg), pp 247–264.
11. Battin TJ, Sengschmitt D (1999) Linking sediment biofilms, hydrodynamics, and river bed clogging: Evidence from a large river. *Microb Ecol* 37:185–196.
12. de Brouwer JFC, Wolfstein K, Ruddy GK, Jones TER, Stal LJ (2005) Biogenic stabilization of intertidal sediments: The importance of extracellular polymeric substances produced by benthic diatoms. *Microb Ecol* 49:501–512.
13. Ascaso C, Wierzchos J, Castello R (1998) Study of the biogenic weathering of calcareous litharenite stones caused by lichen and endolithic microorganisms. *Int Biodeterioration Biodegradation* 42:29–38.
14. Petrich C, Eicken H (2010) Growth, structure and properties of sea ice. *Sea Ice—An Introduction to Its Physics, Biology, Chemistry and Geology*, eds Thomas DN, Dieckmann GS (Blackwell Scientific, London), pp 22–77.
15. Riedel A, Michel C, Gosselin M, LeBlanc B (2007) Enrichment of nutrients, exopolymeric substances and microorganisms in newly formed sea ice on the Mackenzie shelf. *Mar Ecol Prog Ser* 342:55–67.
16. Thomas DN, et al. (2001) Dissolved organic matter in Antarctic sea ice. *Ann Glaciol* 33:297–303.
17. Passow U, Alldredge AL (1995) A dye-binding assay for the spectrophotometric measurement of transparent exopolymer particles (TEP). *Limnol Oceanogr* 40:1326–1335.
18. DuBois M, Gilles KA, Hamilton JK, Reber PA, Smith F (1956) Colorimetric method for the determination of sugars and related substances. *Anal Chem* 28:350–356.
19. Underwood GJC, Fietz S, Papadimitriou S, Thomas DN, Dieckmann GS (2010) Distribution and composition of dissolved extracellular polymeric substances (EPS) in Antarctic sea ice. *Mar Ecol Prog Ser* 404:1–19.

20. Nichols CM, et al. (2005) Chemical characterization of exopolysaccharides from Antarctic marine bacteria. *Microb Ecol* 49:578–589.
21. Raymond JA, Knight CA (2003) Ice binding, recrystallization inhibition, and cryoprotective properties of ice-active substances associated with Antarctic sea ice diatoms. *Cryobiology* 46:174–181.
22. Dickie G (1852) Notes on the algae. *Journal of a Voyage in Baffin's Bay and Barrow Straits in the Years 1850–1851*, ed Sutherland PC (Longman, Brown, Green, and Longmans, London), Vol II, pp cxci–cc.
23. Ibanoglu E (2005) Effect of hydrocolloids on the thermal denaturation of proteins. *Food Chem* 90:621–626.
24. Gosselin M, Legendre L, Therriault J-C, Demers S (1990) Light and nutrient limitation of sea-ice microalgae (Hudson Bay, Canadian Arctic). *J Phycol* 26:220–232.
25. Wettlaufer JS (1998) Introduction to crystallization phenomena in natural and artificial sea ice. *Physics of Ice-Covered Seas: Lecture Notes from a Summer School in Savonlinna, Finland 6–17 June 1994, Helsinki*, ed Leppäranta M (University of Helsinki Department of Geophysics, Helsinki), pp 105–194.
26. De Zoysa DS, Ragusa SR (1995) Biological, chemical and physical factors influencing the seasonal change of polysaccharide concentration in irrigation-channel sediment. *J Appl Phycol* 7:461–470.
27. Kim G (2004) Hydraulic conductivity change of bio-barrier formed in the subsurface by the adverse conditions including freeze–thaw cycles. *Cold Regions Sci Technol* 38:153–164.
28. Marcotte M, Hoshahili ART, Ramaswamy HS (2001) Rheological properties of selected hydrocolloids as a function of concentration and temperature. *Food Res Int* 34:695–703.
29. Hart TD, Chamberlain AHL, Lynch JM, Newling B, McDonald PJ (1999) A stray field magnetic resonance study of water diffusion in bacterial exopolysaccharides. *Enzyme Microb Technol* 24:339–347.
30. Xuewu Z, et al. (1996) Rheological models for xanthan gum. *J Food Eng* 27:203–209.
31. Regand A, Goff HD (2002) Effect of biopolymers on structure and ice recrystallization in dynamically frozen ice cream model systems. *J Dairy Sci* 85:2722–2732.
32. Pertaya N, et al. (2007) Fluorescence microscopy evidence for quasi-permanent attachment of antifreeze proteins to ice surfaces. *Biophys J* 92:3663–3673.
33. Collins RE, Rocap G, Deming JW (2010) Persistence of bacterial and archaeal communities in sea ice through an Arctic winter. *Environ Microbiol* 12:1828–1841.
34. Deming JW, Fortier L, Fukuchi M (2002) The International North Water Polynya Study (NOW): A brief overview. *Deep Sea Res II* 49:1–6.
35. Delille B, Jourdain B, Borges AV, Tison J-L, Delille D (2007) Biogas (CO$_2$, O$_2$, dimethylsulfide) dynamics in spring Antarctic fast ice. *Limnol Oceanogr* 52:1367–1379.
36. Lannuzel D, Schoemann V, de Jong J, Tison J-L, Chou L (2007) Distribution and biogeochemical behaviour of iron in the East Antarctic sea ice. *Mar Chem* 106:18–32.
37. Rysgaard S, Glud RN, Sejr MK, Bendtsen J, Christensen PB (2007) Inorganic carbon transport during sea ice growth and decay: A carbon pump in polar seas. *J Geophys Res* 112:C03016.
38. Freitag J, Dobrindt U, Kipfstuhl S (2002) A new method for predicting transport properties of polar firn with respect to gases on the pore space scale. *Ann Glaciol* 35:538–544.

Supporting Information

Krembs et al. 10.1073/pnas.1100701108

SI Materials and Methods

The source of algal EPS for tank experiments was the diatom *Melosira arctica* var. *krembsii*, isolated from bottom sea ice in the Chukchi Sea near Barrow (71° 20' N, 156° 40' W) in June 2001 (1). Cells were grown to high density at −1.9 °C under light levels of 50 $\mu E \cdot m^{-2} \cdot s^{-1}$ in 2-L beakers containing 0.2 μm-filtered seawater amended with silicate and the nutrients of medium f/2 (2). The cultures were released during January into an insulated, polyethylene-lined, 1,000-L outdoor ice tank (1 × 1 × 1 m with open top) filled with artificial seawater (Instant Ocean, Aquarium Systems), the nutrients of medium f/2, and diatomaceous earth (0.001 $g \cdot L^{-1}$) for continuous supply of silicate. A submerged heating element and two pumps distributed salt, heat, and silicate evenly in the water. The diatoms reached significant (nonaxenic) biomass by March, when subsamples were transferred to indoor 13-L tanks (at −10 °C) and allowed to settle overnight, forming a visible layer at the bottom. The overlying EPS-rich water, called "*Melosira* EPS," was siphoned off for use in ice-growth experiments.

For experiments using xanthan gum (XG), a stock solution of XG (Sigma) at 135 $g \cdot L^{-1}$ in distilled water was first diluted stepwise into a 50-L solution of NaCl, using a commercial-grade blender to prevent clumping. The solution was adjusted to final volume of 200 L and salinity of 30, then sonicated for 30 min.

To prepare "*Colwellia* EPS," *C. psychrerythraea* strain 34H (3) was grown in 2216 marine broth (Sigma) to high optical density in 5-L batch cultures at −1 °C (4). After filtration through 0.7-μm GF/F filters, the EPS-containing filtrate was precipitated overnight in 90% ethanol, resuspended in 100 mL of distilled water, and precipitated again in 90% ethanol. Before use in experiments, the ethanol was removed by evaporation at 90 °C to exclude its effects on ice growth.

To prepare *Melosira* EPS for tests of glycoprotein effects on ice-pore complexity, 700 mL were incubated at 37 °C with glycerol-free *N*-glycosidase F (specific activity ~1,800,000 units·mg^{-1}), an enzyme that hydrolyzes nearly all types of *N*-glycan chains of glycoproteins between the innermost GlcNAc and asparagine residues of high mannose, as well as hybrid and complex oligosaccharides and *N*-linked glycoproteins (5). The glycoprotein fraction was then deactivated for 10 min at 37 °C, using glycoprotein denaturing buffer (0.5% SDS, 1% β-mercaptoethanol) in combination with G7 Reaction Buffer (50 mM sodium phosphate, pH 7.5, at 25 °C), supplemented with 1% Nonidet P-40 (5). Additional volumes of *Melosira* EPS were incubated without the glycosidase for 10 min at 37 °C (enzyme-free control) or at 75 °C (colloid-stabilized control). The latter temperature is considered sufficient to denature most proteins, including glycoproteins (6), unless stabilized by hydrocolloids or gums (7).

1. Kaczmarska I, Jahn R (2006) Taxonomic appraisal of *Melosira arctica* Dickie and description of a new variety (Bacillariophyta). *Botanica Marina* 49:151–164.
2. Guillard RL, Ryther JH (1962) Studies on marine plankton diatoms. I. *Cyclothella nana* Hustedt and *Detonula confercacae* (Cleve) Gran. *Can J Microbiol* 8:229–239.
3. Methé BA, et al. (2005) The psychrophilic lifestyle as revealed by the genome sequence of *Colwellia psychrerythraea* 34H through genomic and proteomic analyses. *Proc Natl Acad Sci USA* 102:10913–10918.
4. Huston AL, Methé B, Deming JW (2004) Purification, characterization, and sequencing of an extracellular cold-active aminopeptidase produced by marine psychrophile *Colwellia psychrerythraea* strain 34H. *Appl Environ Microbiol* 70:3321–3328.
5. Sigma (2004) Biochemicals and reagents for life science research. *Sigma-Aldrich Catalogue 2004–2005* (Sigma-Aldrich, St. Louis), p 1642..
6. Srinivas VR, Singha NC, Schwarz FP, Surolia A (1998) Differential scanning calorimetric studies of the glycoprotein, winged bean acidic lectin, isolated from the seeds of *Psophocarpus tetrogonolobus*. *FEBS Lett* 425:57–60.
7. Ibanoglu E (2005) Effect of hydrocolloids on the thermal denaturation of proteins. *Food Chem* 90:621–626
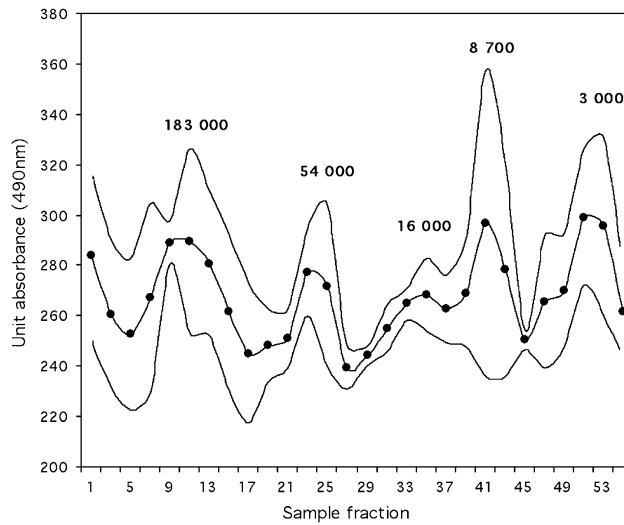
Fig. S1. Mass molecular fractions of total EPS precipitated in ethanol and separated via differences in density in a NaCl and CsCl gradient. The black line represents the average EPS concentration per collected sample fraction of three parallel runs; the gray lines indicate SD ($n = 3$). Following collection, each of the 28 sample fractions was hydrolyzed by the phenol-sulfuric acid method (1). EPS concentration is given as light absorption (490 nm) by the hydrolyzed macromolecules. Numbers above each of the major adsorption peaks are in daltons (a standard unit of molecular mass). Sample fraction 1 indicates an unresolved component of high molecular weight material.

1. Dubois M, Gilles KA, Hamilton JK, Reber PA, Smith F (1956) Colorimetric method for the determination of sugars and related substances. *Anal Chem* 28:350–356.
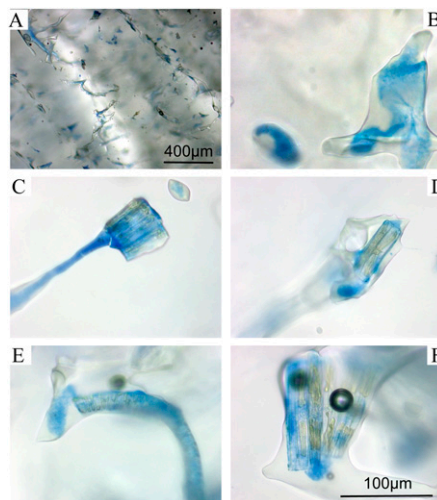
Fig. S2. Photomicrographs at −10 °C of natural sea ice, permeated with Alcian blue stain immediately after collection in March 2002 (*A* and *B*) and in June 2001 (*C–F*), depicting angular (*A*, low magnification) and EPS-filled (*B–F*, high magnification) pores. Pores shown from the June ice also contain diatoms (*C–F*).
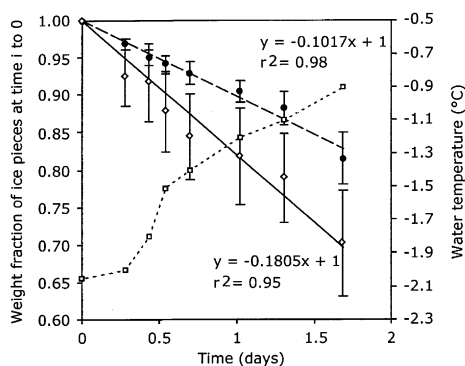
Fig. S3. Evaluation of melting rate of saline ice, with (●) and without (◇) EPS, in a NaCl solution, salinity of 30, that warmed from near freezing at −1.9 °C to −0.9 °C (□) over the 1.7-d incubation period. The decrease in ice mass over time was determined for granular ice pieces (initial volume of 100 mL each) formed either from an EPS-free NaCl solution (◇) or the same solution first amended with XG (40 mg·L^{-1}; ●) under continuous mechanical stirring to achieve uniform XG and salt content (bulk ice salinity of 8). Floating saline ice pieces, with crushed freshwater ice placed among them to prevent lateral convection, were marked with numbers, weighed at each time point (accuracy of 0.02 g), and returned to position. Data points indicate mean (n = 5) fractional weights of ice at time i relative to time 0; error bars indicate SD of the mean.

Table S1. Vertical profiles of size-fractionated EPS in natural sea ice and ice grown in a 13-L tank from saline solution containing *Melosira* EPS*

Depth in ice, cm[†]	AB	PSA			
	pEPS	pEPS	dEPS	tEPS	% pEPS
Natural sea ice, bottom 10-cm section*					
0.00–1.25	9.49	1.99	9.05	11.0	18
1.25–2.50	7.17	3.31	4.63	7.94	42
2.50–3.75	6.84	3.31	5.74	9.05	37
3.75–5.00	10.6	2.65	13.4	16.0	17
5.00–6.25	10.7	2.43	6.73	9.16	26
6.25–7.50[‡]	11.0	2.43	10.9	13.4	18
7.50–8.75	9.71	4.30	10.5	14.8	29
8.75–10.0	9.93	5.52	10.6	16.1	34
Mean	9.5	3.2	8.9	12	28
SD (n = 9)	1.5	1.2	3.0	3.3	9.5
Tank-grown ice[§] with *Melosira* EPS					
0.00–2.50		4.19 ± 1.32	48.2 ± 26.4	52.4	8.1
2.50–5.00		4.74 ± 1.54	49.1 ± 6.29	53.8	8.8
5.00–7.50		2.87 ± 0.33	56.9 ± 18.2	59.8	4.7
7.50–10.0		4.08 ± 1.43	67.2 ± 41.8	71.5	5.8
10.0–12.5		5.29 ± 2.32	64.9 ± 6.18	70.2	7.5
Mean		4.2	57	62	7.0
SD (n = 5)		0.88	8.7	8.9	1.7

*All values, analyzed by the Alcian Blue (AB) or phenol-sulfuric acid (PSA) method, in units of mg·XGequiv·L^{-1}; for individual ice sections containing *Melosira* EPS, values indicate mean ± SD, n = 5; pEPS, >0.4 µm; dEPS, <0.4 µm; tEPS, summed total; means, depth-averaged values.
[†]The lowermost 10-cm section of ice from a 157-cm long core collected in June 2001 near Barrow, AK.
[‡]Horizon of ice selected for detailed microscopic analyses (Figs. 1 and 2).
[§]Over the full thickness (0–12.5 cm) of ice grown in the tank (Fig. 3B); pEPS not determined by the AB method for this ice.

Table S2. Vertical profiles of macronutrients, particulate organic carbon and nitrogen, chlorophyll *a*, phaeopigments, and selected ratios in the bottom 10-cm section of natural sea ice*

Depth in ice section, cm	$Si(OH)_4$	NO_3	NO_2	NH_4	PO_4	POC	PN	Chl*a*	Phaeo	N/P	NO_3/total N	POC/PN	Chl*a*/phaeo
0.00–1.25	0.3	0.2	0.05	9.7	0.3	1.12	0.14	12.4	27.2	35	0.01	7.9	0.46
1.25–2.50	0.6	0.2	0.05	8.7	0.2	1.04	0.12	16.8	38.5	51	0.02	8.7	0.44
2.50–3.75	0.9	0.2	0.05	5.1	0.2	1.14	0.13	12.3	27.7	27	0.03	8.7	0.44
3.75–5.00	0.8	0.2	0.04	3.6	0.2	1.07	0.13	14.3	32.3	24	0.04	8.2	0.44
5.00–6.25	1.2	0.2	0.05	3.9	0.2	1.08	0.13	15.0	33.7	18	0.06	8.5	0.45
6.25–7.50[†]	1.0	0.4	0.05	3.5	0.2	1.05	0.14	17.5	40.8	19	0.09	7.8	0.43
7.50–8.75	0.9	0.4	0.05	2.4	0.3	1.74	0.22	36.7	83.0	10	0.13	7.9	0.44
8.75–10.0[‡]	1.4	1.0	0.05	2.7	0.4	2.21	0.31	55.1	12.3	10	0.27	7.2	4.50

*From a 157-cm core collected in June, 2001 near Barrow, AK; all macronutrients in units of $\mu mol \cdot L^{-1}$, particulate organic carbon (POC) and nitrogen (PN) in units of $mg \cdot L^{-1}$, and chlorophyll *a* (chla) and phaeopigments (phaeo) in units of $\mu g \cdot L^{-1}$.
[†]Horizon of ice selected for detailed microscopic analyses (Figs. 1 and 2), based on its high pEPS and dEPS content (Table S1).
[‡]Ice–water interface and horizon supporting an ongoing diatom bloom (note highest values for POC, PN, Chl*a*, and Chl*a*/phaeo ratio and lowest values for phaeo and POC/PN ratio).

Table S3. Microscopic observations at −10 °C of the visible contents and angularity of brine inclusions* in natural sea ice

Fraction of individual pore space occupied by pEPS	No. of pores (% of total pores) with given fraction of pEPS-occupied space	No. of pores (% of pores with given fraction of pEPS-occupied space) with co-occurring biogenic contents or angularity		
		Diatoms	Detritus	Angularity[†]
0	397 (48)	2 (<1)	12 (3)	108 (27)
¼	131 (16)	7 (5)	20 (15)	57 (43)
½	75 (9)	2 (3)	13 (17)	34 (46)
¾	83 (10)	3 (4)	16 (19)	39 (47)
1	148 (18)	6 (4)	22 (15)	79 (53)
Any fraction[‡]	436[§] (52)	18 (4)	71 (16)	209 (48)

*A total of 834 pores were observed in thin sections cut <3 cm from the ice–water interface in a core collected near Barrow, AK, in June 2001.
[†]Of pores completely filled with stained EPS, 53% were highly angular and convoluted in shape, a frequency that decreased to 43% for pores partially filled with EPS and to 27% for pores devoid of visibly stained EPS.
[‡]Data in this row are the sum of those from all rows for any fraction of individual pore space occupied by pEPS, from 1/4 to fully occupied (1); compare with data in the first row for pores occupied by no visibly stained pEPS (0).
[§]Of these pores containing pEPS, 4% also contained diatoms and 16% also contained detritus; compare with pores devoid of visibly stained pEPS, where 0.5% also contained diatoms and 3% also contained detritus.

Table S4. Vertical profiles of the bulk salinity* of ice grown in 200-L tanks from saline solutions without EPS or with XG or *Melosira* EPS

Ice depth, cm[†]	Control (0)	XG (0.31)	XG (10.3)	XG (194)	*Melosira* EPS (7.9)
0–2.5	10.4 ± 1.6	10.8 ± 0.4	10.6 ± 2.2	11.6 ± 1.3	14.2 ± 1.0
2.5–5.0	5.1 ± 0.2	7.0 ± 0.4	5.1 ± 0.4	7.5 ± 0.9	12.5 ± 0.3
5.0–7.5	7.0 ± 0.5	6.4 ± 1.3	7.1 ± 0.5	8.8 ± 1.4	15.4 ± 0.3
7.5–10.0	8.1 ± 0.7	6.9 ± 0.6	8.2 ± 0.3	9.0 ± 1.8	18.8 ± 0.1
10.0–12.5	9.1 ± 0.7	8.0 ± 0.3	10.6 ± 1.2	9.5 ± 1.0	—
12.5–15.0	10.7 ± 3.2	10.1 ± 0.5	17.3	11.5 ± 1.0	—
15.0–17.5	—	16.1 ± 1.9	—	15.0 ± 0.6	—
Mean[‡]	8.4	9.3	9.8	10.4	15.2
SD (*n* = 4–7)	2.1	3.4	4.2	2.5	2.7

*Values for bulk salinity indicate the mean ± SD (*n* = 3); all values for EPS given parenthetically in units of $mg \cdot XGequiv \cdot L^{-1}$.
[†]At ice-growth rates of 0.25–0.35 $cm \cdot h^{-1}$ in control (no added EPS) and XG tanks and 0.10 $cm \cdot h^{-1}$ in the *Melosira* EPS tank; — indicates no ice grown to this depth.
[‡]Depth-averaged salinity.

Table S5. Bulk salinity and total EPS content* of ice grown in 13-L tanks at −10 °C from seawater solutions amended with *Colwellia* EPS

Ice section, cm	Added *Colwellia* EPS, mg·XGequiv·L^{-1}	Bulk ice salinity	EPS in ice, mg·XGequiv·L^{-1}
0–2.5	0	9.0 ± 0.6	20.0 ± 9.8[†]
	7.4	9.5 ± 0.7	26.5 ± 16.0
	29.5	10.5 ± 0.8[‡]	30.9 ± 22.6
2.5–5.0	0	9.9 ± 0.8[§]	9.8 ± 6.9
	7.4	10.0 ± 0.7	23.8 ± 17.7
	29.5	11.6 ± 0.8[‡§]	37.3 ± 22.8

*Values for bulk salinity and total EPS content indicate mean ± SD ($n = 11$).
[†]EPS in this control ice (no *Colwellia* EPS added) sourced to the sea salts solution, made from Instant Ocean in these experiments.
[‡]Significantly higher than in the comparable ice section grown from the lower starting level of added EPS (*t* test, unequal variances, one-tailed; $n = 11$, $P < 0.05$).
[§]Significantly higher than in the 0- to 2.5-cm ice with comparable starting level of added EPS (*t* test, unequal variances, one-tailed; $n = 11$, $P < 0.05$).